International Journal of Architectural, Civil and Construction Sciences
ISSN: 2415-1734
Vol:12, No:10, 2018

Numerical Investigation for External Strengthening of Dapped-End Beams

A. Abdel-Moniem, H. Madkour, K. Farah, A. Abdullah

Abstract**—**The reduction in dapped end beams depth nearby the supports tends to produce stress concentration and hence results in shear cracks, if it does not have an adequate reinforcement detailing. This study investigates numerically the efficiency of applying different external strengthening techniques to the dapped end of such beams. A two-dimensional finite element model was built to predict the structural behavior of dapped ends strengthened with different techniques. The techniques included external bonding of the steel angle at the re-entrant corner, un-bounded bolt anchoring, external steel plate jacketing, exterior carbon fiber wrapping and/or stripping and external inclined steel plates. The FE analysis results are then presented in terms of the ultimate load capacities, load-deflection and crack pattern at failure. The results showed that the FE model, at various stages, was found to be comparable to the available test data. Moreover, it enabled the capture of the failure progress, with acceptable accuracy, which is very difficult in a laboratory test.

Keywords**—**Dapped-end beams, finite element, shear failure, strengthening techniques, reinforced concrete, numerical investigation.

I. Introduction

PRECAST concrete girders with dapped ends are commonly used in parking structures, pedestrian bridges, and in long-span bridges. Although, dapped ends are useful in reducing the structure's height, two dramatic problems are resulted. The first problem is that the shear stresses at the end of the beam must be carried by a much smaller section. The second one is the stress concentration near re-entrant corner of dapped end that usually produces wide cracks at this area. These cracks increase the danger of damage due to corrosion.

Unfortunately, the mechanism of load transfer through dapped ends is hard to represent using conventional design procedures. Because of these challenges, the design of dapped ends requires special produces [1], [2]. PCI design handbook [3] describes the five potential failure modes for dapped end. These failure modes are caused by flexure and axial tension at the extended end, and direct shear and diagonal tension in the un-dapped portion.

The external strengthening techniques have shown great influence in repairing and strengthening of dapped end beams capacity. Holden et al. [4] experimentally tested precast system that combined post-tensioned unbounded carbon fiber tendons and steel fiber reinforced concrete. Hanson [5] declared the results of testing and estimation of pocketed spandrel beams that included dapped-ends. Huang [6], [7] tested precast pre-stressed concrete double tee members strengthened using FRP composites. They tested two different strengthening techniques ($0^o/90^o$) wrapping and compared them to get a better understanding of the dapped-end behavior and the efficiency of using externally bonded fiber reinforced polymers (FRP) composites.

Valerio [8] used vertical steel and fiber-reinforced plastic bars to be inserted into pre-drilled holes and vaulted in place using epoxy resin for shear strengthening of existing concrete bridges. FRP applied using the externally bonded reinforcement (EBR), or near surface mounted reinforcement (NSMR) techniques have been proven to be efficient for strengthening RC structures [9]-[11]. Gold et al. [12] strengthened with FRP several dapped-end beams of a three-story parking garage that were insufficient in shear capacity. A series of tests were carried out to verify the effectiveness of the FRP strengthening as well as the predictive performance of their design approach.

Taher [13] studied the efficiency of some strengthening techniques for increasing the capacity of dapped-end beams. Tests for 52 rectangular beams showed that the using of FRPs produces the best way for strengthening and retrofitting of dapped end. Using Strut and Tie Method (STM), Taher also estimated the capacity of the FRP-strengthened dapped-end beams. Nevertheless, this model did not take into consideration any size effects of dapped ends.

Tan [14] studied the effectiveness of many FRP arrangements for strengthening dapped-end beams with insufficient shear resistance, consisted of both fiber types and mechanical anchorage systems for FRPs. The results illustrated that the ultimate load increased by 43, 75, 80 percent for carbon fiber plates (CP), carbon fiber sheets (CS), and glass fiber fabrics (GS) systems, respectively. He has also shown that the tested mechanical anchorage devices provided higher profiteering of the FRP systems' strengthening capacity by prohibition their deboning.

Huang and Nanni [15] tested the FRPs capability to improve the capacity of dapped-end beams, and Atta et al. [16] produced an experimental investigation for the torsional behavior of recessed RC beams and studied the application of FRP sheets, FRP laminates and external pre-stressing steel under torsional moments. Gyorgy et al. [17] studied experimentally and numerically the efficiency of strengthening dapped-end reinforced concrete beams using externally bonded carbon FRP.

A. Abdel-Moniem (Master Student) is with the Aswan University, Egypt (e-mail: abdelnasermi@gmail.com).
H. Madkour and K. Farah are with the Structural Engineering Department, Aswan University, Egypt
Abdullah is with the Structural Engineering Department, Aswan University, Egypt and Civil Engineering Department, Bisha University, Saudi Arabia.

II. Scope and Objectives

The main objective of this study is to numerically analyze using ABAQUS 6.10 [18]. Various techniques are used for externally strengthening dapped end beams using different materials. The techniques included external bonding of the steel angle at the re-entrant corner, un-bounded bolt anchoring, external steel plate jacketing, exterior carbon fiber wrapping (CFW) and/or stripping (CFRP), and external inclined steel plates. The numerical results were compared with the experimental results of Taher [13]. In addition, the ultimate capacities were predicted using proposed strut and tie models (STM) for regions for discontinuity (D-regions) related to [13], [19]-[21]. The results were compared with the numerical results to investigate the performance for estimating the failure loads of RC dapped end beams.

III. Finite Element Analysis and Nonlinear Solution Technique

A. Specimen Design and Materials

The dimensions and details of reinforcement for beams under study are illustrated in Fig. 1. The concrete and steel material properties are illustrated in Tables I and II, respectively. While the CFW and carbon fiber reinforced polymers (CFRP) stripping properties are indicated in Table III.

For concrete, concrete damaged plasticity model (CDP) was selected in the present study. The CDP model makes use of the yield function of Lubliner et al. [22], with modifications proposed by Lee and Fenves [23] to account for different evolution of strength under tension and compression. This technique has the potential to represent the inelastic behavior of concrete in both tension and compression [24].

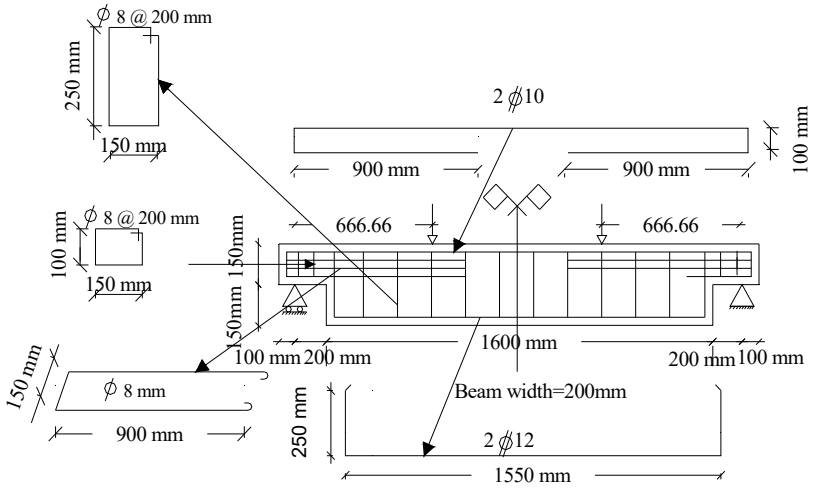

Fig. I1 Dimensions and reinforcement details of modelled beam [13]

TABLE I
Concrete Material Properties for the Proposed Model

Property	Unit	Value
Concrete compressive strength	MPa	2.5
Concrete modulus of elasticity	MPa	22000
Concrete Poisson's ratio	-	0.18
Maximum compressive strain	-	0.003

TABLE II
Steel Material Properties for the Proposed Model

Property	Unit	Value
Yield stress for steel rebars	MPa	400
Ultimate stress for steel rebars	MPa	600
Yield stress for steel stirrups	MPa	280
Yield stress for steel stirrups	MPa	250
Steel modulus of elasticity	MPa	191500
Steel Poisson's ratio	MPa	0.3

For concrete under compression, the material model specified in Eurocode 2, part 1.1 [26], is modified to include the initial linear elastic response up to 40% of the mean compressive strength as shown in Fig. 2 (b). The mean compressive strength ($F_{cm} = F_{ctk} + 8$) of concrete was taken as the peak compressive strength, where (F_{ctk}) is the characteristic compressive strength of concrete, while the tensile behavior of concrete here is represented by an approach applied by Scanlon [27] as shown in Fig. 2 (a).

TABLE III
CFRP, and CFW Material Properties for the Proposed Model [25]

Material	CFRP	CFW
Thickness (mm)	0.13	1.2
Longitudinal modulus of elasticity E_x (MPa)	230000	170000
Laminate Tensile Strength (MPa)	3500	3100
Laminate Elongation at Break in tension	1.56%	1.8%
Density (g/cm^3)	1.82	1.6
Major Poisson's ratio υ_{xy} , υ_{yx}	0.22	0.22

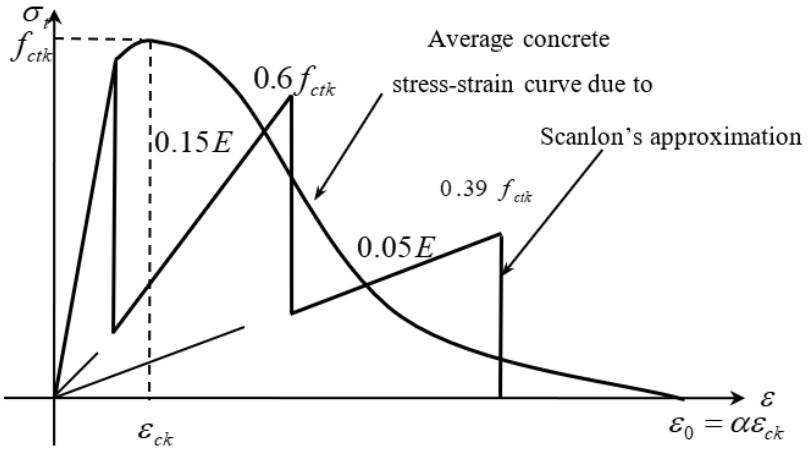

(a)

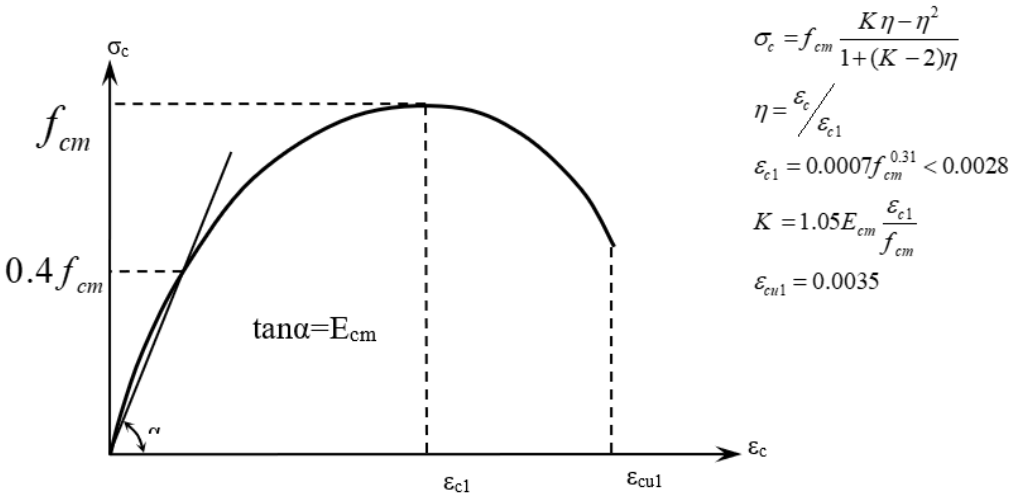

(b)

Fig. 2 Concrete behavior under uniaxial loading in, (a) tension, (b) compression

B. Numerical Analysis

The dapped- end beams represented in this research work as two-dimensional (2D) plane stress continuum element. Due to the beams symmetry, half of the beam length is adopted in the modeling. Finite element software ABAQUS [18] was used to model the concrete beam, adopting a discrete modelling approach. For representing concrete element, we used four-node bilinear plane stress quadrilateral element (CPS4). Each node has two-dimensional translational degrees of freedom.

A two-dimensional two-node linear displacement (T2D2) truss element was adopted to represent the internal steel reinforcements. These truss elements are embedded into "host continuum elements. Embedding means that the translational degrees of freedom at the nodes of the embedded element are eliminated and become constrained to the corresponding interpolated values in the host continuum element. Perfect bond between the grid reinforcement and the surrounding concrete material was assumed.

For modeling the supports of beam (hinged or roller), a two -dimensional rigid shell element was adopted. All elements were connected to a reference point where the boundary conditions were applied as shown in Fig. 3. A conventional layered shell element was selected to model FRP reinforcement. A linear elastic orthotropic constitutive relation was assumed for the CFRP and the carbon fiber warping (CFW).

The mesh was taken square to obtain good results with the test one. It was taken 50*50 mm as shown in Fig. 3 (b), while Fig. 3 (a) shows load and beam boundary condition. In this work, the total load applied was divided into a series of load increments (or) load steps. Newton–Raphson equilibrium iterations provide convergence at the end of each load increment within tolerance limits.

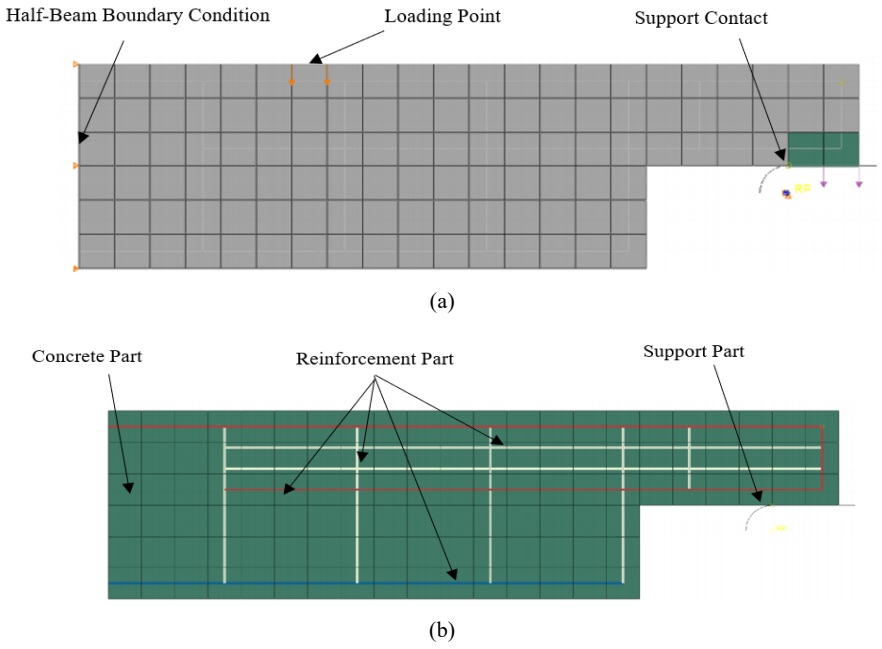

Fig. 3 Beam model (a) model elements, (b) loads and boundary conditions

C. Limitations for Interpreting Failure Modes in the Numerical Modeling

As mentioned before, the studied beams have been modeled as a 2D plain stress problem, together with a smeared approach to model the CFRP sheets and plates, which in turn does not allow for simulation of CFRP debonding from the concrete surface. Hence, the debonding was accounted for indirectly by monitoring the debonding strain in the FRP sheets and the anchorage length. That is, it is hard to predict what type of debonding would occur for these different FRP systems. The debonding strains were determined using the procedures presented in Sas et al. [28] for FRP sheets, and by Chen [29] for steel plates to determine the debonding load for FRP sheets. These bond models are summarized in the following.

1. Bond Model for FRP Plates and Sheets [28]

$$\varepsilon_d = \sqrt{\frac{2G_f}{E_p t_p w}} \quad (1)$$

And the critical bonding length of FRP plate l_{cr}

$$l_{cr} = \sqrt{\frac{E_p t_p}{2f_{ctm}}} \quad (2)$$

where

$$G_F = 0.644 f_c' \quad (3)$$

$$w = \sqrt{\frac{\tau_{max}^2}{2E_p t_p G_f}} \quad (4)$$

$$\tau_{max} = 3.5 f_c'^{0.19} \quad (5)$$

where G_F fracture energy is defined by the stress-slip curve, f_{ctm} is the mean tensile strength of concrete, f_c' is the compressive strength of concrete, E_p is the Young's modulus of elasticity for FRP, t_p is the thickness of FRP sheet or plate, τ_{max} is the maximum shear stress at interface, and ε_d is the debonding strain.

For each type of FRP, the debonding strain (ε_d) is estimated as illustrated in Table IV. These parameters are used to estimate the debonding load, which was considered to occur when the debonding strain, which was developed over the entire width of the CFRP, was recorded at the location of the calculated anchorage length.

2. Bond Model for EBR Steel Plates [29]

$$\varepsilon_b = \frac{\sigma_p}{E_p} \quad (6)$$

$$\sigma_b = 0.427 \beta_p \beta_L \sqrt{\frac{E_p \sqrt{f_c'}}{t_p}} \quad (7)$$

$$\beta_p = \sqrt{\frac{2 - b_p/b_c}{1 + b_p/b_c}} \quad (8)$$

$$\beta_L = \begin{bmatrix} 1 & if\ L \geq L_c \\ \sin\frac{\pi L}{2 L_c} & if\ L \leq L_c \end{bmatrix} \quad (9)$$

$$L_c = \sqrt{\frac{E_p t_p}{\sqrt{f_c'}}} \quad (10)$$

where σ_p is the stress in bonded plate at failure, L_c is the effective bond length, L is the bond length.

III. Numerical Program

27 reinforced concrete dapped-end beams were modeled numerically. The beams have various strengthening techniques; 12 specimens of them are based on [13], while other specimens were proposed through the current investigation. The strengthening systems used in this study are based on five potential modes of failure for dapped end that are described in PCI [3].

Several materials and layouts were used in the numerical investigation, as shown in Figs. 4 and 5. The specimen number B.A.J, subscript A is the number of beam series C, D, E, F, H, I, K, L, M, N, O, P, S; subscript J is the number of beams REF., 1, 2, 3, 4, 5, 6. The beams with subscript (REF.) have previous experimental results from the literature [13]. The strengthening techniques used are:

i. Steel plate angle 50*50*3 mm epoxy-glued and positioned at the re-entrant corners to control the diagonal tension and direct shear cracks therein (B-C-REF.).
ii. Unbounded inclined threaded steel bolt in drilled hole (USB) 12 mm diameter is aligned in 45 degree to control inclined cracks within its line of action (B- D-REF.), while beam (B-D-1) the inclination angle became 52^0. Two and three rows of inclined bolts have been applied for beams from (B-D-2) to (B-D-5) as shown in Fig. 5.
iii. A combination of unbounded inclined threaded steel bolts in drilled hole (USB) 12 mm diameter aligned in 45 degree and steel plate 50*50*3 mm.
iv. Steel plate jacketing (SPJ/1) 600 mm length and 1 mm thickness (B-H-REF.). Steel plate jacketing (SPJ/2) 600 mm length & 1mm thickness (B-I-REF.). Steel plate jacketing (SPJ/3) 200 mm length & 1mm thickness (B-K-REF.). While beams (B-H-1) and (B-I-1) pate length was increased by 150 mm, and 200 mm for beam (B-K-1) to study the effect of length on limiting the diagonal tension cracks.
v. Exterior 0.13 mm CFW-Sikawrap [25] aligned horizontally in the extended ends with 600mm length on each side (B-N-REF.), both extended and dapped ends with 600 mm length on each side (B-L-REF.) and vertically in the reentrant zones only with 200 mm width (B-O-REF.), thus providing equivalent external horizontal or vertical reinforcement.
vi. Inclined CFRP-Sikacarbodur S512 [25] stripping of 1.2 mm thickness and 25 mm total width and aligned at 450 to control the inclined cracks within its line of action (B-P-REF.),
vii. Combination of CFRP stripping and CFW described in the latter two categories thus presenting specimens (B-F-REF.), (B-R-REF.), (B-S-REF.), respectively, for more control of the diagonal tension cracks.
viii. Inclined steel plate with 1.2 mm thickness 50 mm width and aligned at 45 degree (B-M-1), two and three rows (B-M-2), (B-M-3), aligned 52 degree (B-M-4), two rows one at nib and one at full depth with 50 and 100 mm width (B-M-5), (B-M-6) to compare with inclined CFRP stripping.

IV. Results and Discussion

A. Load - Deflection Relationship

Fig. 6 illustrates different external steel techniques. The steel plate jacketing method is a suitable technique for improving the behavior of dapped end, as shown in Fig. 6 (B-I-REF.). By comparing it with the external angle and inclined bolt, because it has the best load capacity, besides it has a great effect on the limiting of the shear cracks in the recess corner compared with external angle and inclined bolt methods.

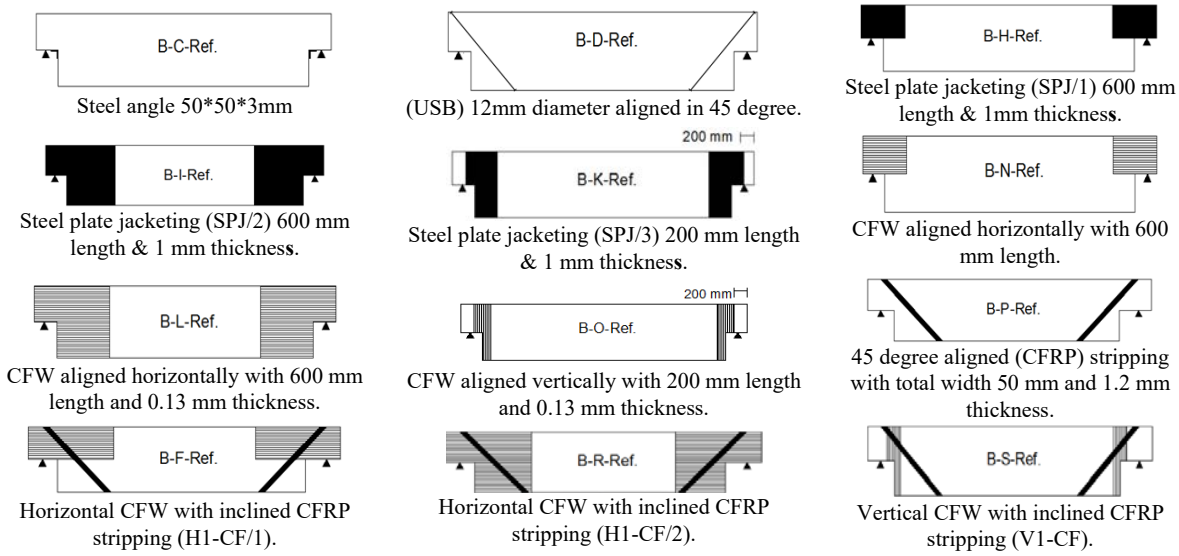

Fig. 4 Different dapped-end strengthening techniques proposed by Taher [13]

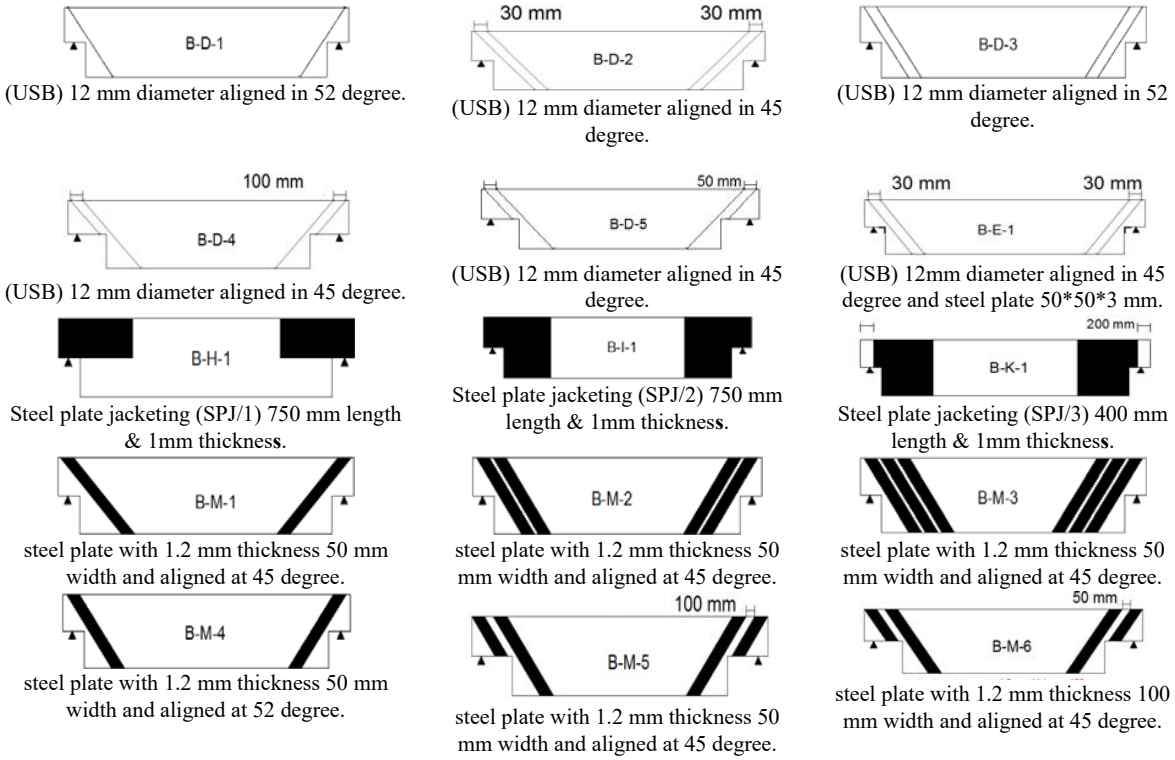

Fig. 5 Various strengthening techniques modelled numerically

The bolt anchoring method shown in Fig. 6, for specimen (B-D-REF), presented the better ductile behavior. The mode of failure for it is tensile failure initiated by yielding of hanger bars, while the other specimens have sudden modes of failure mainly dominated by brittle shear failure. In addition, cracks were evolving until abrupt deboning occurred for other external plates or sheets strengthening techniques. This was followed by unexpected modes of failure fundamentally predominated by brittle shear failure.

The change in inclination angle of bolt from 45° to 52° has no salient change in load capacity. The use of two-inclined bolts instead of one bolt also has no effect on the dapped end behavior or capacity as shown in Tables IV and V. On the other hand, steel angle method has a little increase in load capacity, whereas the use of a combination of two inclined steel bolts aligned at 45 degree and steel plate 50*50*3 mm is a more effective technique as shown in Fig. 6. The load capacity increased by 18% with an increase in maximum deflection while Fig. 7 illustrates the effect of increasing the length of the plate behind the reentrant corner on the behavior of dapped end. The load-deflection curve shows that the capacity foe specimens with 750 mm are bigger than specimens with 600 mm length.

Specimens (B-M-6) that have two-inclined steel plates one at full depth and the other at nib depth as shown in Fig. 5 achieved the best behavior. These results illustrate the importance of putting the plate closed to re-entrant corner as possible, it is preferred to use two-closed one at nib depth, and the other at full depth as illustrated in Table V.

While Fig. 8 shows the effect of using CFW, and inclined carbon fiber polymers (CFRP) on the strengthening of dapped-end region. From the results of load deflection curve, we can see that it is recommended to use horizontal CFW in both the reduced and full depth zones with inclined CFRP stripping as shown for specimen (B-R-Ref).

The initial behavior was nearly linear until first cracking, with almost the same inclination for all specimens. The largest load carrying capacity was found to be exhibited by specimens (B-D-Ref) and (B-I-Ref) then (B-D-Ref) followed by (B-R-Ref). While the maximum deflection was noted in beam (B-S-Ref) then beam (B-L-Ref) followed by (B-D-Ref).

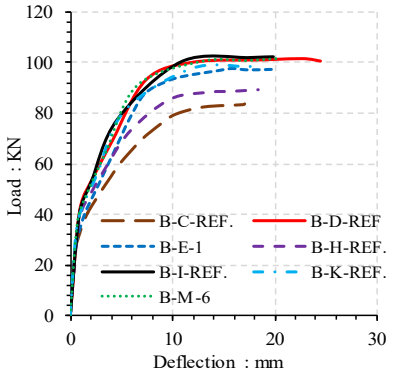

Fig. 6 Load- deflection curve for angle, bolt, and steel plate strengthening methods

Generally, the load-deflection curves for the beams from

present finite element analysis agree to a large degree with the previous experimental data [13]. Despite, the finite element loads are partially different from the experimental capacity. Differences are due to some reasons. First, micro cracks are present in the concrete for the tested beam and could be produced by drying shrinkage in the concrete and/or handling of the beam. While the finite element models do not include the micro cracks. Another reason is the proposed perfect bond between the concrete, external strengthening, and steel-reinforcing bars in the finite element analysis. This assumption would not be true for the tested beam.

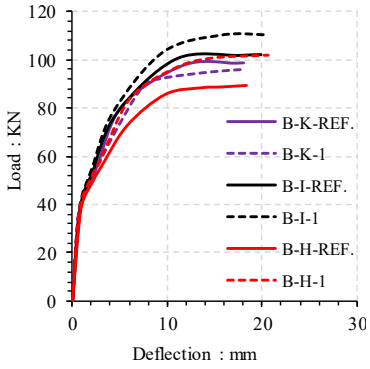

Fig. 7 Load- deflection curve for specimens strengthened with different steel plate jacketing layouts

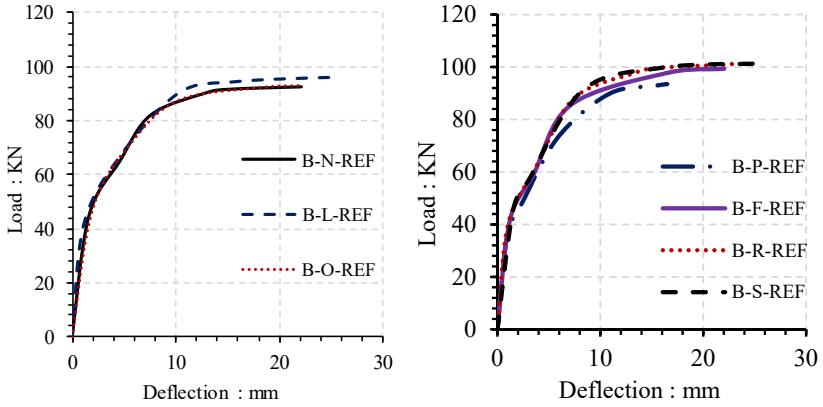

Fig. 8 Load- deflection curve for specimens strengthened with horizontal and vertical CFW, inclined CFRP stripping only, and a combination of CFRP with CFW

B. Cracking and Ultimate Loads

Table IV illustrates cracking load, ultimate load, maximum flexural strain of reinforcement, and maximum concrete strain at the cracking nib for specimens presented in Fig. 4. In addition, ultimate load was estimated analytically by using strut and tie model based on [13], [19]-[21], and then compared with the experimental [13] and numerical results, while cracking load, ultimate load, maximum flexural strain of reinforcement at the bottom and the maximum cracked nib concrete strain are measured numerically as illustrated in Table V for specimens of Fig. 5.

The analysis by the numerical program produced results with an average difference about 8% from the experimental observations. While the strut and tie model proposed in [13], [19]-[21] always introduce lower load values than the numerical results, because it depends on the first tie yield or first strut crush.

For steel plate jacketing technique, Specimen (B-I-Ref) has the largest ultimate capacity because it has an adequate length behind the recess zone. Then, specimen (B-K-Ref) is less than (B-I-Ref) because the developed length behind the re-entrant corner is smaller. While (B-H-Ref) is the least in the ultimate capacity because the plate shape could not prevent both shear cracks at reentrant corner and diagonal tension cracks at full depth.

The increase in length of steel plate leads directly to increase in load capacity of dapped end beam as illustrated in Tables IV and V. For example, the increase in total plate length of beam (B-H-Ref) from 600 mm to 750 mm leads to rise in ultimate load by 14% and by 7.2% for specimen (B-I-Ref), whereas the ultimate load increased by 12% due to the increase in total length from 200 mm to 400 mm for specimen (B-K-Ref).

The use of plate aligned in $45°$ increased ultimate capacity by 17% to the control beam (beam without strengthening), and by the same percentage for plate aligned with $52°$ (specimens B-M-1 & B-M-4), whereas putting two closed plates increased the ultimate capacity by 19.79%, and by 21.67% for three closed steel plates (specimens B-M-2 & B-M-3). In addition, use of two-inclined steel plates one at full depth and the other at nib depth as shown for specimens (B-M-5 & B-M-6) leads to an increase in the ultimate capacity by 18.68%, and 26.41% respectively, and the shear cracks for these are less than specimens from (B-M-1) to (B-M-4). These results illustrate that the best technique is to put two-closed inclined plates one at nib depth and the other at full depth.

The use of horizontal CFW in nib with length 600 mm (B-N-REF.) gave the same ultimate capacity and maximum

deflection as vertical CFW (B-O-REF.) as illustrated in Table IV. In addition, the same ultimate strains values for concrete and flexural reinforcement were achieved. While the use of horizontal CFW extended in nib depth and full depth area, as shown in the specimen (B-L-Ref) is better than specimens (B-N-Ref), and (B-O-Ref). This may be due to the ultimate capacity and deflection of this specimen which is larger than the two other specimens

Table IV illustrated that the combination of CFW and inclined CFRP stripping (B-F-Ref), (B-R-Ref), and (B-S-Ref) gave a better capacity than use of each strengthening technique alone. The ultimate capacity increased by 7.44% for first specimen (B-F-Ref), by 5.55% for second (B-R-Ref), and by 9.2% for the third (B-S-Ref) in compared with specimens (B-N-Ref), (B-L-Ref), and (B-O-Ref), respectively.

C. Crack Pattern

The crack patterns sketch obtained from present finite element analysis at the predicted failure loads of specimens (B-R-Ref.) are shown in Fig. 9. The figures illustrate the direction of the tensile equivalent elastic strain, its vector is normal to crack plan. It can be observed that numerous cracks occur at mid span of finite element model at any load level. The cracks begin at the re-entrant corner of the dapped end beams at load level 40 kN, as the load is further increased, additional cracks form and existing cracks lengthen. Then, cracks are spread in recess, end and flexural cracks are appearing in the mid span followed by shear cracks at support and inclined shear cracks in recess end until failure at a load of 101.28 kN. The diagonal tension crack in nib assumes a flatter trajectory on reaching the hanger reinforcement, propagating to the loading point. That failure mode agrees with experimental mode of failure and with the simulation of struts (concrete), and ties (the tension steel bars with almost constant stress) modelling for deep beam, and corbel.

TABLE IV
A COMPRESSION BETWEEN EXPERIMENTAL [13] AND NUMERICAL RESULTS

Beam	Cracking load P_{cr} (kN)			Ultimate load P_u (kN)			Comparison of ultimate load	
	EXP	Numerical	%Numerical /EXP	EXP	Numerical	STM	% Numerical /EXP	% STM / EXP.
B-C-Ref.	44	30	68	76	83.50	56.29	109	148
B-D-Ref.	40	29.05	72	92	101.40	64.16	110	155
B-H- Ref.	45	34	75	81	89.05	63.15	109	128
B-I-Ref.	43	30	69	94	102.04	63.15	108	148
B-K-Ref.	43	27.70	64	78	98.50	63.15	126	123
B-N-Ref.	39	39.3	100	87	92.47	47.83	106	180
B-L-Ref.	38	39	102	96	95.95	47.83	99	200
B-O-Ref.	31	39	125	85	92.74	78.39	109	108
B-P-Ref.	35	35.83	102	89	93.51	89.36	105	99
B-F-Ref.	41	41.07	100	93	99.35	89.36	106	104
B-R-Ref.	37	40	108	99	101.28	89.36	102	110
B-S-Ref.	35	40	114	90	101.28	89.36	112	100
			AVG				108	133
			Standard Deviation (S)				6	13.6
			Coefficient of Variation (COV)				0.059	0.1

Debonding Strain (10-3)	Ultimate Plate Strain (10-3)	Debonding Load (kN)	% Increase in Load at Main Steel Yielding	Max. nib cracked Concrete strain (E-003)
-	-	-	8.57	13.1
-	-	-	20.71	14.2
-	2.5[c]	-	9.57	17.9
1[a]	3.3[c]	102.04[e]	14.29	14.9
-	6.8[c]	-	12.29	10.3
6[b]	11[d]	92.47[f]	16	15
6[b]	15[d]	95.95[f]	11.29	15.8
6[b]	15[d]	59.35[f]	11.29	15.3
3[b]	5[d]	56.1[f]	7.86	9.73
3[b]	6.2[d]	48.07[f]	18.57	13.12
3[b]	6[d]	62.64[f]	19.86	14.09
3[b]	6.5[d]	46.74[f]	19	14.81

- Exp. = the experimental load from the literature [13], Numerical = the numerical load calculated in this study, STM = the corrected strut-tie model load according to [13], [19]-[21].
- [a] Debonding strain for steel plates is calculated by (6), [b] Debonding strain for FRP is calculated by (1).
- [c] Ultimate strain for steel plates, and [d] Ultimate strain for FRP have been calculated numerically by using ABAQUS [18].
- [e] Debonding load for steel plates, [f] Debonding load for FRP (the load corresponding to the debonding strain) have been calculated numerically by using ABAQUS [18].
- % Increase in Load at Main Steel Yielding is the ratio between yielding load for main steel at bottom for each beam to yielding load for the reference beam (beam without strengthening)
- Max. Nib cracked Concrete strain is the total concrete strain for the beams at the re-entrant corner of the dap.

TABLE V
NUMERICAL RESULTS FOR THE ADDITIONAL STRENGTHENING SYSTEMS

Beam	Cracking load P_{cr} (kN)	Ultimate load P_u (kN)			Debonding Strain (10-3)	Ultimate FRP Strain (10-3)	Debonding Load (kN)	% Increase in Load at Main Steel Yielding	Max. nib cracked Concrete strain (E-003)
		Numerical	STM	% Numerical / STM					
B-D-1	29	101.07	71.29	141	-	-	-	21.14	10.2
B-D-2	31.25	103.44	128.33	80	-	-	-	13.86	13.4
B-D-3	29.60	102.88	143.61	71	-	-	-	20.71	11.8
B-D-4	31.25	101.95	64.16	158	-	-	-	14.29	15
B-D-5	30.72	102.85	64.16	160	-	-	-	20.71	11.1
B-E-1	30	98.91	128.33	77	-	-	-	19.71	12.3
B-H-1	34.5	101.63	63.15	160	1[a]	2.6[c]	65.13[e]	14.29	18.8
B-I-1	31.5	110.48	63.15	174	1[a]	3.7[c]	109.48[e]	17.57	19.3
B-K-1	27.70	109.39	63.15	173	-	3.4[c]	-	15.71	12
B-M-1	40.50	94.33	47.65	197	2[a]	9[c]	35.84[e]	10.57	10.9
B-M-2	40.50	96.41	95.31	101	2[a]	6.8[c]	47.24[e]	14.29	10.2
B-M-3	40	97.92	95.31	102	2[a]	5.2[c]	47.5[e]	14.79	9.53
B-M-4	40	94.01	53.34	176	2[a]	9.2[c]	40.42[e]	14.00	10.9
B-M-5	40.50	95.52	95.31	100	2[a]	9.2[c]	39.15[e]	10.57	10.8
B-M-6	43	101.74	95.31	106	-	3.7[c]	-	22.14	12

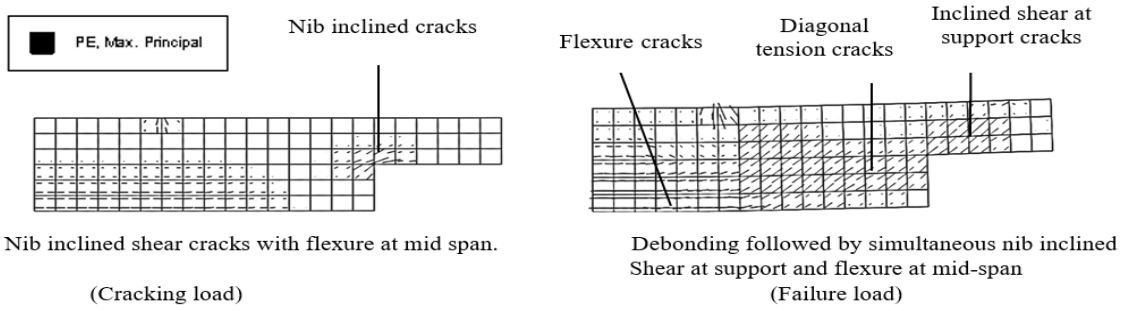

Fig. 9 Numerical predictions of crack pattern for specimen (B-R-Ref)

TABLE VI
A COMPARISON BETWEEN THE NUMERICAL AND THE EXPERIMENTAL MODES OF FAILURE

Beam	Mode of Failure	
	Experimental	Numerical
B-C-Ref.	Ripping off in recess zone followed by shear compression.	Ripping off in recess zone followed by shear compression.
B-D-Ref.	Bolt yielding followed by flexure at mid-span.	Bolt yielding followed by flexure at mid-span. And shear compression failure
B-H-Ref.	Debonding followed by vertical direct shear crack at reentrant corner.	Flexural and shear cracks in the full depth zone
B-I-Ref.	Debonding followed by vertical direct shear crack at reentrant corner.	Debonding followed by flexural and shear cracks in the full depth zone
B-K-Ref.	Debonding followed by vertical direct shear crack at reentrant corner.	vertical direct shear crack at reentrant corner.And flexural cracks in full depth
B-M-1		Nib inclined cracks with diagonal tension cracks and flexural cracks in the full depth
B-N-Ref	Debonding followed by nib inclined shear at support. Flexural shear cracks were noted in the full depth zone	Debonding followed by nib inclined shear at support. Flexural shear cracks were noted in the full depth zone
B-L-Ref B-O-Ref	Debonding followed by nib inclined shear at support.	Debonding followed by nib inclined shear at support. Flexural shear cracks were noted in the full depth zone
B-P-Ref	Peeling followed by simultaneous nib inclined shear at support and flexure at mid-span.	Debonding followed by nib inclined shear at support and flexure at mid-span.
B-F-Ref	Peeling followed by nib inclined shear at support and flexure at mid-span.	Debonding followed by nib inclined shear at support and flexure at mid-span.
B-S-Ref	Peeling followed by nib inclined shear at support.	Debonding followed by nib inclined shear at support and flexure at mid-span.

Experimental, is the experimental mode of failure from the literature [13].

D. Mode of Failure

A comparison between the numerical mode of failure and the previous experimental mode of failure from the literature [13] is made as shown in Table VI. All of beams strengthened by steel plate jacketing method and CFW technique have failed by debonding of the plates or sheets with inclined shear cracks at the recess end. The beams (B-P-Ref), (B-F-Ref), and

(B-S-Ref), have failed due to debonding of inclined carbon fiber stripping with shear at recess end and flexural cracks at mid span.

The biggest tensile strains in reinforcement for all beams were found near the re-entrant corner at the longitudinal reinforcement. Just before failure of all specimens, the main reinforcement and the stirrups in the shear span were yielded. Numerical results showed that the strengthening methods had not become effective before first cracking. The results of the crack pattern illustrated that the using of external CFW and steel plate jacketing (SPJ/2) have a great effect on the limiting of the shear cracks in the recess corner compared with other strengthening techniques.

V. Conclusions

A Finite element model has been developed to simulate the behavior of reinforced concrete dapped-end beams under static monotonic loading. The model takes into account the linear and nonlinear material properties for concrete as well as steel reinforcement. The FE model was compared with the results of previous experimental beams to have a good verification. The predicted loads and the modes of failure of the reinforced concrete dapped-end beams by the present FE models at various stages were found to be in good agreement with the previous test data.

This study numerically investigated the different external strengthening techniques that often used to increase the load capacity of dapped ends. Twenty-seven specimens with eight different strengthening techniques were modelled. From that, the following conclusions are drawn:-

a. In this study, numerical model was found to provide better prediction of ultimate load for dapped end beams compared to strut and tie models.
b. The steel plate jacketing method is a suitable technique for improving the behavior of dapped end. Because it has the best load capacity, besides it has a great effect on the limiting of the shear cracks in the recess corner compared with external angle and inclined bolt methods. While the bolt anchoring technique presented the better ductile behavior.
c. Externally FRP strengthening technique was found to be a suitable method to strength of dapped end beams especially the use of horizontal CFW in both the reduced and full depth zones with inclined CFRP stripping. Because it could develop a high ductility and strength after the concrete cracked.
d. From the studied techniques, the best serviceability behavior was achieved by using two-closed inclined steel plates one at nib depth, and the other at full depth (B-M-6). Because it has the maximum cracking load and the maximum increase percent in yielding load for the main reinforcement.
e. The maximum ultimate capacity was achieved by using Steel plate jacketing (SPJ/2) in nib and full depth with a total length larger than twice of nib length (B-K-1). Because it gives the maximum ultimate loads between all other beams.

References

[1] R. Herzinger, "Stud reinforcement in dapped ends of concrete beams," presented at the AICSGE 5, At Alexandria, Egypt 2008.
[2] A. H. Mattock and T. Theryo, *Strength of Members With Dapped Ends*: Prestressed Concrete Institute, 1986.
[3] P. I. H. Committee, "PCI design handbook: precast and prestressed concrete," ed: MNL-120. 6th ed. Chicago, IL: PCI, 2006.
[4] T. Holden, J. Restrepo, and J. B. Mander, "Seismic performance of precast reinforced and prestressed concrete walls," *Journal of Structural Engineering,* vol. 129, pp. 286-296, 2003.
[5] J. Hanson, "Testing and Evaluation of Pocketed Spandrel Beams," *Department of Civil, Construction, and Environmental Engineering, North Carolina State University, North Carolina, USA,* 2001.
[6] P.-C. Huang, "Dapped-end strengthening of precast prestressed concrete double tee beams with FRP composites," MS thesis, Univwesity of Mossouri-Rolla, 2000.
[7] P. C. Huang, Myers, J.J., and Nanni, A,. (2000). *Dapped-end strengthening of precast prestressed concrete double tee beams with FRP composites*.
[8] P. Valerio and T. J. Ibell, "Shear strengthening of existing concrete bridges," *Proceedings of the Institution of Civil Engineers-Structures and Buildings,* vol. 156, pp. 75-84, 2003.
[9] T. Fib Bulletin, "Externally bonded FRP reinforcement for RC structures," ed: International Federation for Structural Concrete Switzerland, 2001.
[10] N. R. Council, "Guide for the design and construction of externally bonded FRP systems for strengthening existing structures," *CNR-DT200,* 2004.
[11] A.-. Committee, "Guide for the design and construction of externally bonded FRP systems for strengthening concrete structures," *ACI-440.2 R-02. Farmington Hills: American Concrete Institute,* 2002.
[12] W. J. Gold, G. J. Blaszak, M. Mettemeyer, A. Nanni, and M. D. Wuerthele, "Strengthening dapped ends of precast double tees with externally bonded FRP reinforcement," in *Advanced Technology in Structural Engineering*, ed, 2000, pp. 1-9.
[13] S. Taher, "Strengthening of reentrant corner zone in recessed RC beams," in *Eleventh International Colloquium on Structural and Geotechnical Engineering*, 2005.
[14] K. H. Tan, "Shear strengthening of dapped beams using FRP systems," in *FRPRCS-5: Fibre-reinforced plastics for reinforced concrete structures Volume 1: Proceedings of the fifth international conference on fibre-reinforced plastics for reinforced concrete structures, Cambridge, UK, 16–18 July 2001*, 2001, pp. 249-258.
[15] P.-C. Huang and A. Nanni, "Dapped-end strengthening of full-scale prestressed double tee beams with FRP composites," *Advances in Structural Engineering,* vol. 9, pp. 293-308, 2006.
[16] A. M. Atta and T. F. El-Shafiey, "Strengthening of RC dapped-end beams under torsional moment," *Magazine of Concrete Research,* vol. 66, pp. 1065-1072, 2014.
[17] T. Nagy-György, G. Sas, A. Dăescu, J. A. Barros, and V. Stoian, "Experimental and numerical assessment of the effectiveness of FRP-based strengthening configurations for dapped-end RC beams," *Engineering structures,* vol. 44, pp. 291-303, 2012.
[18] U. m. ABAQUS, "Version 6.10.," in *ABAQUS Documentation*, ed.
[19] A. Committee, A. C. Institute, and I. O. f. Standardization, "Building code requirements for structural concrete (ACI 318-14) and commentary," 2014.
[20] D. H. Sanders, "Dapped-end T-beam supported by an inverted T-beam," *Special Publication,* vol. 208, pp. 91-104, 2002.
[21] J. Schlaich, "Design and Detailing Using Struts-and-Tie Models," *Proc. JCI Int. Wrokshop on Shear in Concrete Structures,* 1994.
[22] J. Lubliner, J. Oliver, S. Oller, and E. Onate, "A plastic-damage model for concrete," *International Journal of solids and structures,* vol. 25, pp. 299-326, 1989.
[23] J. Lee and G. L. Fenves, "Plastic-damage model for cyclic loading of concrete structures," *Journal of engineering mechanics,* vol. 124, pp. 892-900, 1998.
[24] A. M. Abdullah and C. Bailey, *Analysis of repaired/strengthened RC structures using composite materials: punching shear*: University of Manchester, 2010.
[25] SAE., *Technical Information Handbook. Sika Egypt for Construction Chemicals Co*. California, USA, 2003.
[26] B. EN, "1-2: 2004 Eurocode 2: Design of concrete structures-Part 1-2: General rules-Structural fire design," *European Standards, London,*

2004.
[27] A. Scanlon and D. W. Murray, "Time-dependent reinforced concrete slab deflections," *Journal of the Structural Division,* vol. 100, 1974.
[28] G. Sas, A. Carolin, and B. Täljsten, "A model for predicting the shear bearing capacity of FRP-strengthened beams," *Mechanics of Composite Materials,* vol. 44, pp. 245-256, 2008.
[29] J. Chen and J. Teng, "Anchorage strength models for FRP and steel plates bonded to concrete," *Journal of structural engineering,* vol. 127, pp. 784-791, 2001.